

The key factors which determine the cooling effect of blood flow near ultrasonically heated bone.

G. J. Vella¹, **V. F. Humphrey**², **F. A. Duck**³ and **S. B. Barnett**⁴

¹ School of Biomedical Sciences, The University of Sydney, Australia.

² Institute of Sound and Vibration Research. University of Southampton. Southampton .UK.

³ Medical Physics Department, Royal United Hospital Bath, Bath. UK.

⁴ Honorary Research Associate, School of Biomedical Sciences, The University of Sydney, Australia

e-mail of corresponding author: g.vella@fhs.usyd.edu.au

Abstract To determine the critical factors that produce cooling, a phantom simulating human fetal skull bone was immersed in a soft tissue mimicking material (TMM). This was exposed to clinically relevant pulsed Doppler ultrasound with power outputs of up to 255 mW. Water flowing in a 2-mm wall-less channel in the TMM, at various distances from the bone target, simulated blood flow. The temperature was measured at the inner surface of the bone. The cooling effect was more effective as the distance between the perfusing channel and bone was decreased, as the number of channels increased and as the ultrasound beamwidth increased.

Introduction

Pulsed Doppler ultrasound is often used in obstetrics to determine blood flows in a fetal brain such as in intracranial arteries [1]. As this mode of ultrasound generally requires enhanced power levels to penetrate some areas of skull bone, due to its high ultrasonic absorption coefficient [2], there is the potential to produce temperature rises of over 5 °C [3] in tissues close to bone. This raises an important safety issue for central nervous tissue, which animal studies have shown is sensitive to temperature elevations of 4.5 °C above normal for a few seconds [4]. Whilst blood flow in tissue (i.e. perfusion) is acknowledged to produce a measure of cooling [5], the extent and nature of this cooling is not fully understood.

A number of animal studies have been carried out to assess the effects of blood flow on the ultrasound-induced heating in fetal or neo-natal skull bone. An accepted method of achieving this was to measure the temperature elevation during ultrasonic exposure while the animal was alive and again immediately after the animal was euthanased. The difference in the maximum temperature rise in skull bone gave a measure of the cooling due to perfusion. Measurements using different animal models have obtained varying amounts of perfusion-induced cooling from 0 to 43%, depending on the location at which the temperature was measured and the width of the ultrasonic beam used [6], [7]. Hence it is desirable to use a simple and reproducible skull bone-brain tissue phantom to investigate the critical factors that determine the cooling effect of a single large vessel or a number of smaller vessels, without the complication of differing conditions.

The aim of the present study is twofold: 1. To fabricate a simple test phantom with ultrasonic properties similar to a human fetal head; 2. to measure the cooling effect of water flowing at a steady rate in a simulated artery or channel near an ultrasonically heated bone target as a function of ultrasonic source power, flow rate, bone-channel separation distance, ultrasonic beamwidth and number of perfusing channels.

Methods and Materials

A phantom was fabricated, which simulated a human fetal brain and skull bone. The ‘skull bone’ (0.5 mm thick) was made from a high-density polyethylene which has similar thermal

and ultrasonic properties as human fetal bone. The ‘brain tissue’ was made from an animal gelatine and water mixture [8] of tissue mimicking material (TMM).

Perfusion was simulated by allowing water to flow (at room temperature) in a single 2-mm diameter wall-less channel in the TMM material at various distances from the bone target. Figure 1 shows the key features of the bone phantom. Another experiment used 4 channels, each of diameter 1.4 mm and yet another used 8 channels, each of diameter 0.5 mm. A flow rate was produced by a constant pressure head and was maintained by a peristaltic pump, which returned the water to an upper reservoir, as described in greater detail elsewhere [7].

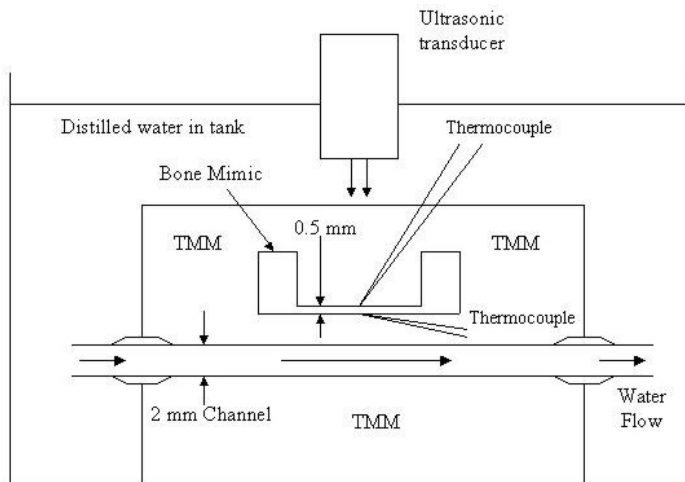


Figure 1. A schematic diagram of the key features of the laboratory constructed bone phantom.

The phantom was exposed to clinically relevant pulsed Doppler ultrasound conditions. A focussed transducer with a centre frequency of 3.5 MHz was used, which emitted pulses of duration $5.7 \mu\text{s}$ with a repetition frequency of 8 kHz and power outputs of up to $255 \pm 5 \text{ mW}$. The pulsing conditions used in this study were chosen to avoid non-linear propagation conditions, which may produce additional heating [9]. Two ultrasonic (-6 dB) beamwidths were used at a power output of $100 \pm 2 \text{ mW}$; 3.1 mm (narrow beam) and 7.8 mm (wide beam) with intensities of $1.1 \text{ W cm}^{-2} \text{ ISPTA}$ and $0.26 \text{ W cm}^{-2} \text{ ISPTA}$, respectively. The temperature was measured with $50 \mu\text{m}$ chromel-alumel thermocouples attached to both surfaces of the bone mimic. In this paper, only the measurements at the surface distal to the ultrasonic transducer are recorded, simulating the inner aspect of a fetal skull.

Results

The cooling effect due to arterial perfusion at a fixed distance from the heated bone surface was found to be independent of the ultrasonic source power for different perfusion rates. Figure 2 illustrates this independence for a bone-channel distance of 1.5 mm.

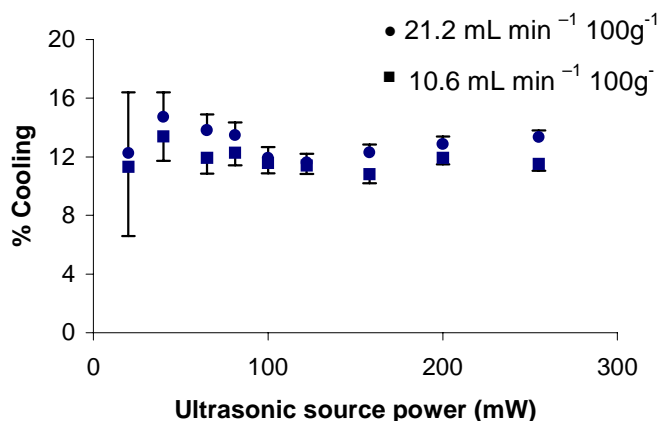


Figure 2. The percentage cooling as a function of ultrasonic source power as measured at the distal surface of the bone surface for two perfusion rates. The error bars represent the standard error of the mean (SEM) of the measurements.

The perfusion-induced cooling effect initially increases with flow rate but then saturates to a constant value (beyond 5 mL/min/100g) dependent on how far the perfusing channel is from the heated bone target (Figure 3). The human fetal cerebral perfusion rate is assumed to be 20 to 30 mL/min/100g, which is well above the saturation value that occurs at approximately 5 mL/min/100g [7]. The error bars represent the SEM of the measurements.

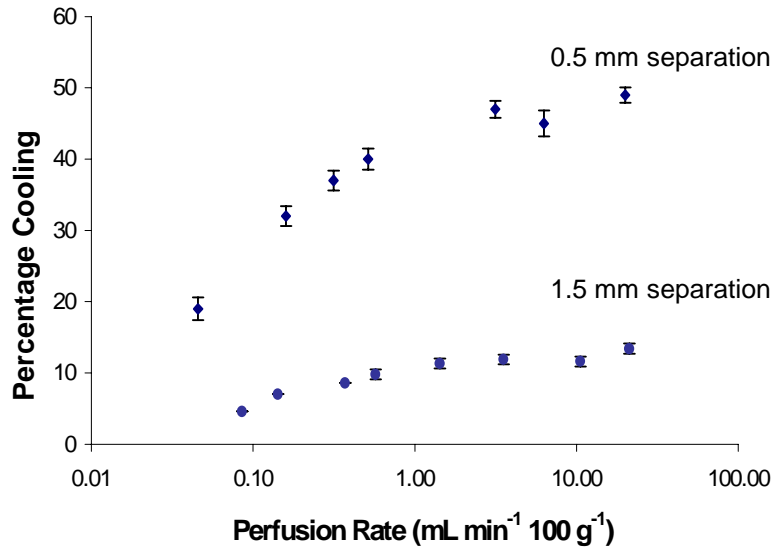


Figure 3. The percentage cooling as a function of the perfusion rate for bone-channel spacings of 0.5 mm and 1.5 mm. In both cases, the specimens were exposed to a narrow ultrasound beam of power 100 mW.

The perfusion-induced cooling effect is strongly dependent on the distance between the perfusing channel and the heated bone target. Furthermore, this cooling effect was more pronounced when a wide ultrasonic beam (compared to a narrow beam) heated the bone. The % cooling by a single perfusing channel after 2 minutes of narrow and wide beam exposure as a function of bone-channel distance, measured at the bone surface distal to the transducer, is shown in Table 1 when the ultrasonic source power was 100 mW.

Table 1. The % cooling as a function of the bone-channel spacing after bone is exposed to a 2-minute exposure to an ultrasonic beam of power 100 mW.

| Bone – Channel Spacing (mm) | % Cooling | |
|-----------------------------|--------------------------------|------------------------------|
| | Narrow Beam (3.1 mm beamwidth) | Wide Beam (7.8 mm beamwidth) |
| 1 | 36.7 ± 1.4 | 49.8 ± 0.8 |
| 1.5 | 13.4 ± 1 | 16.8 ± 0.9 |
| 1.7 | 10.4 ± 1.4 | - - - |
| 2 | 8.1 ± 1.8 | - - - |
| 3 | 3.8 ± 1.9 | 5 ± 1.9 |

The perfusion-induced cooling was enhanced (Table 2) by increasing the number of perfusing channels from 1 to 4, even though the perfusion rate in both were identical, at 23 mL min⁻¹ 100 g⁻¹. In the 4-channel specimen, all channels are in a plane at a separation of 1.3 mm from the distal bone surface. The closest comparative single-channel specimen was the bone-channel separation of 1.5 mm. For the 8-channel specimen, the average distance of the channels from the bone surface was 4 mm. The closest comparative single-channel specimen

was that with a bone-channel spacing of 3 mm. The perfusion rate for both the single and 8 channel cases was above $5 \text{ mL min}^{-1} 100 \text{ g}^{-1}$, the value above which there is no additional cooling due to perfusion [7].

Table 2. Comparison of the percentage cooling for one or more channels as a function of ultrasound beamwidth.

| Number of channels (separation distance) | % Cooling | |
|---|-----------------------------------|---------------------------------|
| | Narrow Beam (3.1 mm beamwidth) | Wide Beam (7.8 mm beamwidth) |
| Single (1.5 mm) | 12.7 ± 1.3 | 16.8 ± 0.9 |
| 4 Channels (1.3 mm) | 15.5 ± 0.8 | 26.3 ± 0.6 |
| Single (3.0 mm) | 3.8 ± 0.3 | 5.0 ± 1.4 |
| 4 Channels (4.0 mm) | 8.3 ± 0.3 | 15.4 ± 1.6 |

For both narrow and wide ultrasonic beams, the multiple channel phantoms produce significantly greater cooling than a single channel at a similar spacing. Furthermore, this cooling is enhanced even further if the multiple channel specimens are exposed to a wide ultrasonic beam as against a narrow beam.

Conclusions

It is acknowledged that the cooling effect of homogeneous *in vivo* perfusion is not the same as cooling by a single large vessel or a number of fine vessels as used in this study. Nevertheless, it has confirmed and strengthened previous findings of both animal experiments and computer simulations. Furthermore, this study has established the following key points when an ultrasound beam heats a bone target. The cooling effect of liquid flow in a single simulated arterial vessel is strongly dependent on how far it is from the bone surface; the closer it is to the bone surface, the more effective the cooling. Perfusion in multiple channels produces a greater cooling than a single channel with the same flow rate. The perfusion-induced cooling is enhanced as the ultrasonic beamwidth, incident on the bone, is increased. The cooling effect of liquid flow in a simulated arterial vessel is independent of the ultrasonic source power. Furthermore, the cooling effect of the liquid flow increases with flow rate but then saturates, at approximately $5 \text{ mL min}^{-1} 100 \text{ g}^{-1}$, to a constant value.

References

- [1] L.M. McCowan & P.M. Duggan, *Early Hum. Dev.*, **30**, 249, (1992)
- [2] F.A. Duck, *Physical properties of tissue, a comprehensive reference book*. London: Academic Press, 1990
- [3] S.B. Barnett, *Ultrasound Med. Biol.*, **27**, 883, (2001)
- [4] M.J. Edwards, K. Shiota, M.S.R. Smith & D.A. Walsh, *Reprod. Toxicol.*, **9**, 411, (1995)
- [5] A. Shaw, R.C. Preston, D.R. Bacon, *Ultrasound Med. Biol.*, **22**, 203, (1996)
- [6] G.J.Vella, V.F. Humphrey, F.A. Duck, S.B. Barnett, *Ultrasound Med. Biol.*, **29**, 779, (2003)
- [7] G.J.Vella, V.F. Humphrey, F.A. Duck, S.B. Barnett, *Ultrasound Med. Biol.*, **29**, 1193, (2003)
- [8] J.Wu, J.D. Chase, Z. Zhu, T.P. Holzapfel. *Ultrasound Med. Biol.*, **18**, 495, (1992)
- [9] D.R. Bacon & E.L. Carstensen, *J. Acoust. Soc. Am.*, **88**, 26 (1990)

agreement between theory and experiment has been obtained for the excited states but not for the ground states. We have now extended the experimental investigations for boron with $\mathbf{B}||\langle 110 \rangle$ and B up to 18 T in the Faraday configuration.

Experimental Results and Discussion

The Zeeman components of the G line [11] of boron in Ge for $\mathbf{B}||\langle 110 \rangle$ are shown in Fig. 1 for a number of values of B, while Fig. 2 gives the spectrum for B = 12 T on a magnified scale. These spectra were all obtained with an unapodised resolution of 0.18 cm^{-1} . In the Faraday configuration \mathbf{E} is perpendicular to \mathbf{B} , where \mathbf{E} is the electric field of the far-infrared radiation. For $\mathbf{B}||\langle 110 \rangle$, the point group, O_h , of the unperturbed impurity reduces to C_{2h} and the irreducible representations of the fourfold degenerate impurity states, Γ_8^\pm , yield $2(\Gamma_3^\pm + \Gamma_4^\pm)$ [9, 10], where the \pm signs are parity labels. These two pairs of Zeeman states will be designated as 3.1, 3.2, and 4.1, 4.2. Transitions from the even-parity ground state to the odd-parity excited states are labelled by (i,f), where $i, f = 3, 4$ and the selection rules are $i = f$ for $\mathbf{E}||\mathbf{B}$ and $i \neq f$ for $\mathbf{E} \perp \mathbf{B}$. Thus eight components are allowed in the present case, all of which are observed. The labelling of the components in Fig. 2 follows the above notation, their identification being based on a comparison with the lower-field, higher-resolution studies for aluminium in Ge [8].

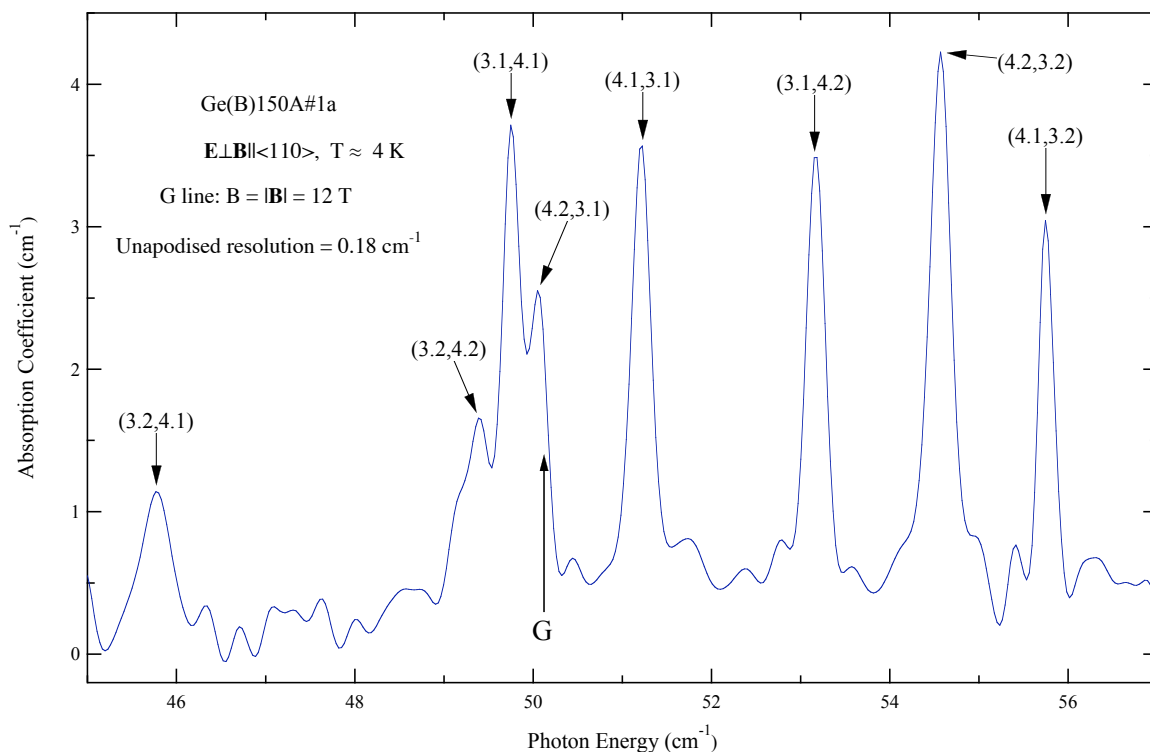


Fig 2. The Zeeman spectrum of the G line of Boron in Germanium at 12 T for $\mathbf{B}||\langle 110 \rangle$ in the Faraday configuration.

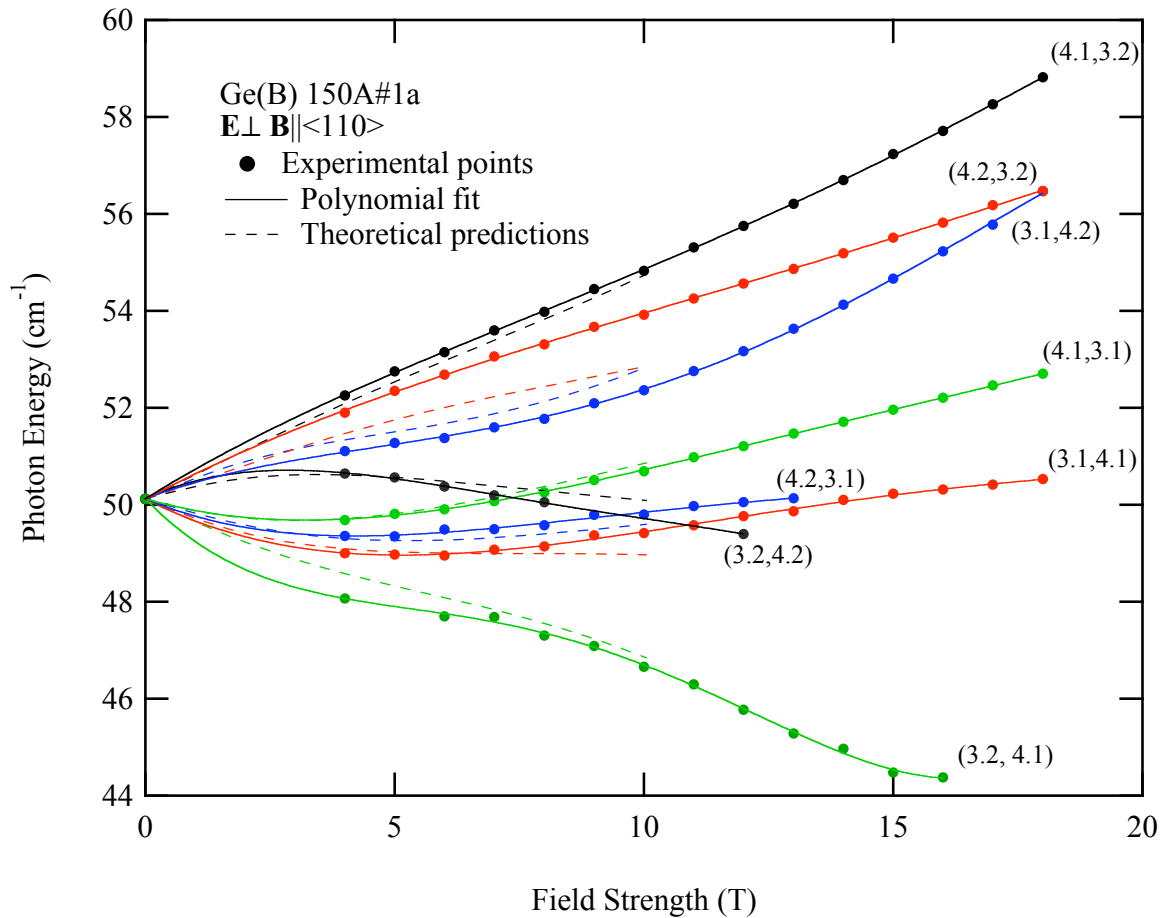


Fig 3. Dependence of the energies of the Zeeman components of the G line of Boron in Ge on magnetic field strength.

In Fig. 3 is given the dependence of the experimental energies of the G components on B. These results are represented by the data points through which the full curves are fitted. Also shown on this figure as dashed curves are the predictions of one of the calculations [10]. It is seen that qualitatively the predictions are in good agreement with the experimental results. However, quantitatively, the experimental and theoretical results for the transition (4.2,3.2) are significantly different.

Conclusions

The qualitative splittings of some of the states involved in the Zeeman spectrum of the G line can be recognised from the labels on the transitions in Figs. 2 and 3. Thus, it is seen that the splitting of the ground states $\Gamma_{3.1}^+$ and $\Gamma_{3.2}^+$ at large magnetic fields is comparable to the splitting of its excited-state counterparts $\Gamma_{3.1}^-$ and $\Gamma_{3.2}^-$ while this is not so for $\Gamma_{4.1}^+$ and $\Gamma_{4.2}^+$. The details of these splittings will be presented elsewhere along with the results of the analysis of the Zeeman data for the other lines obtained in the present studies.

Acknowledgements

We thank D. Smirnov for his experimental expertise. This work was supported by the Australian Research Council and the University of Wollongong. A part of the work was performed at the National High Magnetic Field Laboratory, which is supported by NSF Cooperative Agreement No. DMR-9527035 and by the State of Florida. The boron-doped Ge ingot was provided by the Department of Physics, Purdue University

References

- [1] G. J. Takacs, R. E. M. Vickers, P. Fisher and C. A. Freeth, *Materials Science Forum* **117 & 118**, 123 (1993).
- [2] P. Fisher, G. J. Takacs, R. E. M. Vickers and A. D. Warner, *Phys. Rev. B* (Rapid Commun.) **47**, 12999 (1993).
- [3] R. J. Baker, P. Fisher, C. A. Freeth, D. S. Ryan and R. E. M. Vickers *Solid State Commun.* **93**, 353 (1995).
- [4] G. J. Takacs, PhD Thesis, University of Wollongong (1999).
- [5] R. J. Baker, P. Fisher, R. E. M. Vickers, E. E. Haller and W. L. Hanson, *Shallow-Level Centers in Semiconductors*, eds. C. A. J. Ammerlaan and B. Pajot (World Scientific, Singapore, 1997), p. 357.
- [6] M. A. Horniman, Honours Thesis, University of Wollongong (1997).
- [7] R. J. Baker, P. Fisher, C. A. Freeth, M. A. Horniman, D. S. Ryan, G. J. Takacs, R. E. M. Vickers and A. D. Warner, *Proc 24th. Int. Conf. Phys. Semiconds*, Editor D. Gershoni (World Scientific, 1999) p. 1365.
- [8] R. J. Baker, PhD Thesis, University of Wollongong (2001).
- [9] J. Broeckx, *Phys. Rev. B* **43**, 9643 (1991).
- [10] W. O. G. Schmitt, E. Bangert and G. Landwehr, *J. Phys.: Condens. Matter* **3**, 6789 (1991).
- [11] R. L. Jones and P. Fisher, *J. Phys. Chem. Solids* **26**, 1125 (1965).